AGU PUBLICATIONS

Water Resources Research

RESEARCH ARTICLE
10.1002/2014WR016223

Special Section:
Connectivity, Non-Linearity, and Regime Transitions in Future Earthscapes

The emergence of topographic steady state in a perpetually dynamic self-organized critical landscape

Liam Reinhardt[1] and Michael A. Ellis[2]

[1]Department of Geography, University of Exeter, Penryn, UK, [2]British Geological Survey, Nottingham, UK

Abstract We conducted a series of four physical modeling experiments of mountain growth at differing rates of uplift and three distinct climates ranging from relatively wet to relatively dry. The spatial and temporal pattern of landscape behavior is characterized by $\sim f^{-1}$ scaling in sediment discharge and power law scaling in the magnitude and frequency of ridge movement in all four experiments. We find that internally generated self-organized critical (SOC) processes generate dynamically stable catchment geometries after $\sim$1 relief depths of erosion: these regularly spaced catchments have an average outlet-spacing ratio of 2.16, well within the range of values reported in field studies. Once formed, large catchment bounding ridges oscillate about a critically balanced mean location, with occasional large-scale changes in catchment size. Ridge movement appears to be driven by the competition for discharge as landslides push ridges back and forth. These dynamics lead to the emergence of a complex twofold scaling in catchment dynamics that is fully established by 1.8 relief depths of erosion; at this stage, a clear threshold has emerged separating two distinct scaling regimes, where large ridge mobility is insensitive to relief and small ridge mobility is relief dependent. Overall, we demonstrate that the development of dynamically stable large-scale landforms is related to the emergence of a complex-system hierarchy in topographic dynamics. Once formed, these landscapes do not evolve; statistical properties such as average topography and discharge become stationary while topography remains highly dynamic at smaller length scales.

Key Points:
- Evolving landscapes reveal topography that is both dynamic and steady state
- Evolving topography is a self-organized critical process
- SOC in evolving landscapes is probably related to the activity of landslides

Correspondence to:
M. A. Ellis,
michael.ellis@bgs.ac.uk

Citation:
Reinhardt, L., and M. A. Ellis (2015), The emergence of topographic steady state in a perpetually dynamic self-organized critical landscape, *Water Resour. Res.*, *51*, 4986–5003, doi:10.1002/2014WR016223.

Received 30 JUL 2014
Accepted 13 MAY 2015
Accepted article online 18 MAY 2015
Published online 1 JUL 2015

1. Introduction

This paper explores the internal system dynamics of a simple experimental physical landscape that simulates the development of a high-relief mountainous topography. Our initial goal was to develop findings by *Hasbargen and Paola* [2000, 2003] and *Hasbargen* [2003] in which dynamic topography was recognized in a model landscape that was at flux steady state. A novel addition to our experimental apparatus is the ability to capture sediment discharge at high-temporal resolution in concert with the acquisition of high-spatial resolution digital elevation models. These additional facilities allowed us to explore the parallel development of erosional topography and sediment discharge, and we present the results in the context of a system that shows both self-organized criticality (SOC) as well as the emergence of a complex dynamic topography.

Numerical modeling of mountain landscapes has until recently tended to produce steady state landscapes with fixed topography (with the notable exceptions of *Densmore et al.* [1998] and *Ellis et al.* [1999]) while physical models invariably report a highly dynamic ridge topography even at mass-flux steady state [*Hasbargen and Paola*, 2000, 2003; *Lague et al.*, 2003; *Bonnet and Crave*, 2006; *Bonnet*, 2009; *Paola et al.*, 2009]. More recent numerical efforts that explicitly treat ridge migration as a process interaction with fluvial dynamics have been able to reproduce these physical results [*Goren et al.*, 2014; *Willett et al.*, 2014]. In this paper, we further explore ridge dynamics and show how stable topography can arise at some scales while remaining dynamic at other scales.

The idea that stable structures can emerge in landscapes at different scales is embedded in complexity theory. Complexity theory has as many definitions as it has advocates [*Werner*, 1995, 1999; *Baas*, 2002; *Coco and Murray*, 2007; *Murray and Fonstad*, 2007; *Murray*, 2007; *Murray et al.*, 2009; *Keiler*, 2011] but at its heart it posits that many types of apparently complicated landscapes can be simplified into a small number of important components that exist and interact at distinct spatial and temporal scales. Paradoxically this simplification arises through the collective behavior of many small-scale components, with many degrees of

freedom, that synthesize into effectively new structures and behaviors [*Murray*, 2007; *Murray et al*., 2009]. In this world-view, a hierarchy of scales exist: at each scale, emergent components act to limit the degrees of freedom of the process that created it, hence the simplification, e.g., windblown sand with many degrees of freedom form larger-scale sand dunes, which then act to limit the behavior of sand blowing across them [*Werner*, 1995, 1999]. Each of the new emergent components can in turn interact to create yet larger-scale (emergent) behaviors [*Murray et al*., 2009].

Self-organized critical landscapes are balanced "at the edge of chaos" [*Bak et al*., 1987; *Bak*, 1996]. In theory, even the smallest external forcing can produce a cascade of responses across all scales, implying that SOC landscapes are highly sensitive to external perturbations. It has also been argued that the internal dynamics and negative feedbacks within such systems will tend to dampen signals from external climatic and tectonic perturbations such that they disappear within the general system noise, i.e., SOC systems are insensitive to external forcing [*Coulthard and Van de Wiel*, 2007; *Murray et al*., 2009; *Jerolmack and Paola*, 2010]. To distinguish between these scenarios of high or low sensitivity to external forcing, it is necessary to first quantify the nature and magnitude of the internal dynamics in such a system.

SOC processes dominate channel and high-relief hillslope processes, but it is not clear if these processes create critically balanced landscapes. The problem lies in the numerical models used to simulate, and understand, this type of behavior. *Sapozhnikov and Foufoula-Georgiou* [1996] argued that numerical surface process models contain insufficient degrees of freedom to simulate SOC behavior. Physical models on the other hand, while limited in the number of processes that they simulate, are not limited in degrees of freedom; indeed there are no constraints beyond the physical dimensions of the experimental material and apparatus [*Paola et al*., 2009]. Thus, physical models may be used to complement numerical models in determining whether high-relief landscapes are SOC; this is one of the aims of our paper. *Coulthard and Van de Wiel* [2007] argued that the identification of SOC requires an explanation of how such behavior may arise. In general, this requires identification of the mechanism(s) for a "*chain of failures*" to propagate through a system [*Coulthard and Van de Wiel*, 2007]. The key processes driving (unglaciated) high-relief mountain development are landsliding and channel sediment discharge. Mechanisms for SOC behavior have been identified in a range of channel processes including sediment transport [*Coulthard and Van de Wiel*, 2007; *Van de Wiel and Coulthard*, 2010], riverbank stability [*Fonstad and Marcus*, 2010], and channel avulsions [*Sapozhnikov and Foufoula-Georgiou*, 1997; *Jerolmack and Paola*, 2007]. Less well studied are nonchannelized hillslopes, which researchers often ignore on the basis that hillslopes only account for a small proportion of topographic relief (10–20%): channel networks make up the remainder, hence the focus on them [e.g., *Whipple et al*., 1999]. Contrary to this view, field and numerical modeling studies have shown that hillslopes and ridges can adjust in response to climate change independently of network (base-level) forcing [*Pelletier et al*., 1997; *Gabet et al*., 2004; *Korup et al*., 2010; *Singh et al*., 2015]. Moreover, hillslopes and channels are interdependent both in terms of sediment dynamics and form while ridges set the boundaries within which channel networks function [*Brunsden and Thornes*, 1979; *Brunsden*, 1993; *Fernandes and Dietrich*, 1997; *Korup et al*., 2007, 2010; *Goren et al*., 2014; *Michaelides and Singer*, 2014]. It is therefore important that we quantify the internal dynamics of hillslopes and ridges if we are to understand entire landscapes.

In the physical models of *Hasbargen and Paola* [2000, 2003], *Hasbargen* [2003], and *Lague et al*., [2003], ridges were observed to be highly dynamic, although the cause was not quantified. In such high-relief landscapes, hillslope erosion is dominated by landslides [*Burbank et al*., 1996; *Montgomery and Brandon*, 2002; *Korup et al*., 2007, 2010]. Landsliding is a classic SOC process [*Hergarten and Neugebauer*, 1998; *Malamud and Turcotte*, 1999], characterized by scale-invariant power law frequency-magnitude relationships [*Hovius et al*., 1997; *Malamud and Turcotte*, 1999; *Stark and Hovius*, 2001; *Malamud et al*., 2004; *Hurst et al*., 2013]. Importantly, landslides are also a key mechanism by which catchment bounding ridges move laterally in high-relief landscapes; they do so by altering ridge slope, relief and form [*Korup*, 2006; *Korup et al*., 2007, 2010]. What is less clear is how ridge movement affects fluvial landscape structure [*Goren et al*., 2014; *Willett et al*., 2014].

The "*natural scale independence*" of mountain landscapes makes them highly amenable to physical modeling [*Schumm et al*., 1987; *Hasbargen and Paola*, 2000, 2003; *Hancock and Willgoose*, 2001; *Lague et al*., 2003; *Bonnet and Crave*, 2003, 2006; *Bonnet*, 2009; *Paola et al*., 2009; *Graveleau et al*., 2012; *Rohais et al*., 2012]. Convergent drainage networks follow well-defined self-similar patterns [*Rodriguez-Iturbe and Rinaldo*, 1997; *Jerolmack and Paola*, 2007]. Similarly, mountain topography as a whole commonly follows self-organized self-similar patterns [*Hallet*, 1990; *Rodriguez-Iturbe and Rinaldo*, 1997; *Murray*, 2007]. For example, the ridge-

and-valley topography of mountain catchments displays a striking regularity as defined by near-constant ratios in mountain range width to outlet-spacing (termed the spacing ratio) [*Hovius*, 1996; *Talling et al*., 1997; *Perron et al*., 2008]. Moreover, the SOC nature of the processes previously discussed means that they are scale-invariant over a wide range of scales. Taken together these findings imply that mountain landscapes are scale independent: small copies of the whole are externally similar copies of large mountain systems and operate in much the same way [*Paola et al*., 2009]. It follows that small physical models of mountain landscapes are dynamically scaled models of real mountain environments, albeit with a simplified set of physical process, making them ideal for exploring complex-system dynamics in a laboratory setting.

We conducted a series of four analogue (physical) modeling experiments. In order to draw comparisons between each experiment and to allow comparisons with the real world we focused on relief as the primary topographic attribute. There are two fundamentally different types of erosive landscape with distinct geomorphological controls on landscape-scale erosion rates. In low-relief, low-gradient tectonically inactive mountain belts, hillslope processes set the pace of landscape lowering. In such environments erosion rates increase linearly with relief, as relief strongly correlates with mean slope and the rate of nonglacial erosive processes increases with hillslope gradient [*Gilbert*, 1909; *Ahnert*, 1970; *Montgomery and Dietrich*, 1994; *Summerfield and Hulton*, 1994]. In contrast, erosion rates increase nonlinearly with relief in high-relief tectonically active mountain belts as erosion is accomplished primarily through landsliding. In common with previous experiments of this type [e.g., *Bigi et al*., 2006], landslides were observed to occur frequently in our experiments and it is these type of landscapes that we simulate here.

2. Methodology

We simulated the development of mountainous topography through the slow erosion of a uniform substrate made of a ~20 μm ground quartz paste (Figure 1). We ran four experiments with uplift rates (U) of 9, 30, 40, and 60 mm h^{-1} enabling us to explore a range of topographies. The mean rate of precipitation ranges between 71 and 78 mm h^{-1} (see Table 1). We choose these precipitation and uplift parameters after careful observation of the conditions that produced realistic topographies in silica paste. For example, at $U = 80$ mm h^{-1} massive landslides dominate erosion and fluvial drainage networks fail to become established. Similarly, at very slow uplift rates or relatively high precipitation rates topography is subdued and did not generate the attributes of high-relief mountainous landscapes. The uniform *lowering* of base-level by two weirs on opposite sides of an erosion box simulated mountain *uplift* (Figure 1). Precipitation was delivered through an ultrafine sprinkler system ~1 m above the eroding surface. Our experimental setup is similar in principle to that used by previous authors [*Lague et al*., 2003; *Bonnet and Crave*, 2006].

Precipitation was generated by a system of 20 sprinklers that delivered water droplets with a diameter small enough to avoid any splash dispersion at the surface of the model. The rate and pattern of precipitation was controlled by varying water pressure and the use of nine fans mounted above the sprinklers: see Appendix A for an assessment of the stability of precipitation in these experiments. Topography was measured over the entire model area via a purpose built laser scanner mounted over the apparatus; we cropped each scan 10 mm inward from the weirs and 2.5 mm in from the sidewalls to minimize the potential effect of model boundaries. This laser system has a horizontal precision of <0.6 mm but raw data were gridded to produce a digital elevation model (DEM) with a pixel size of 1 mm. The evolving topography was monitored in 5 min intervals via an overhead digital camera.

Sediment discharge, Q_s, was measured throughout each experiment using two custom built "dischargeometers" mounted on each side of the apparatus. These dischargeometers are measuring cylinders in which the volume between two electronic sensors is known and into which a mix of pure quartz sediment and water flows; the mass between these two sensors is weighed and the cylinder emptied every Δt (typically 30–45 s depending on flow rate). Sediment volume within the filled cylinder, V_s, is calculated as

$$V_s = (M_{sw} - \rho_w V_c)/(\rho_s - \rho_w) \ \ (\mathrm{cm}^3) \tag{1}$$

where M_{sw} is the mass of the sediment-water mixture in the cylinder $= \rho_w V_w + \rho_s V_s$ (g), V_c is the calibrated volume of the cylinder $= V_w + V_s$ (cm^3), V_w is the volume of water in the measuring cylinder (cm^3), ρ_s = sediment density (2.65 g cm^{-3}), and ρ_w = water density (g cm^{-3}). Sediment discharge, Q_s, is then given by $V_s/\Delta t$ (cm^{-3} min^{-1}).

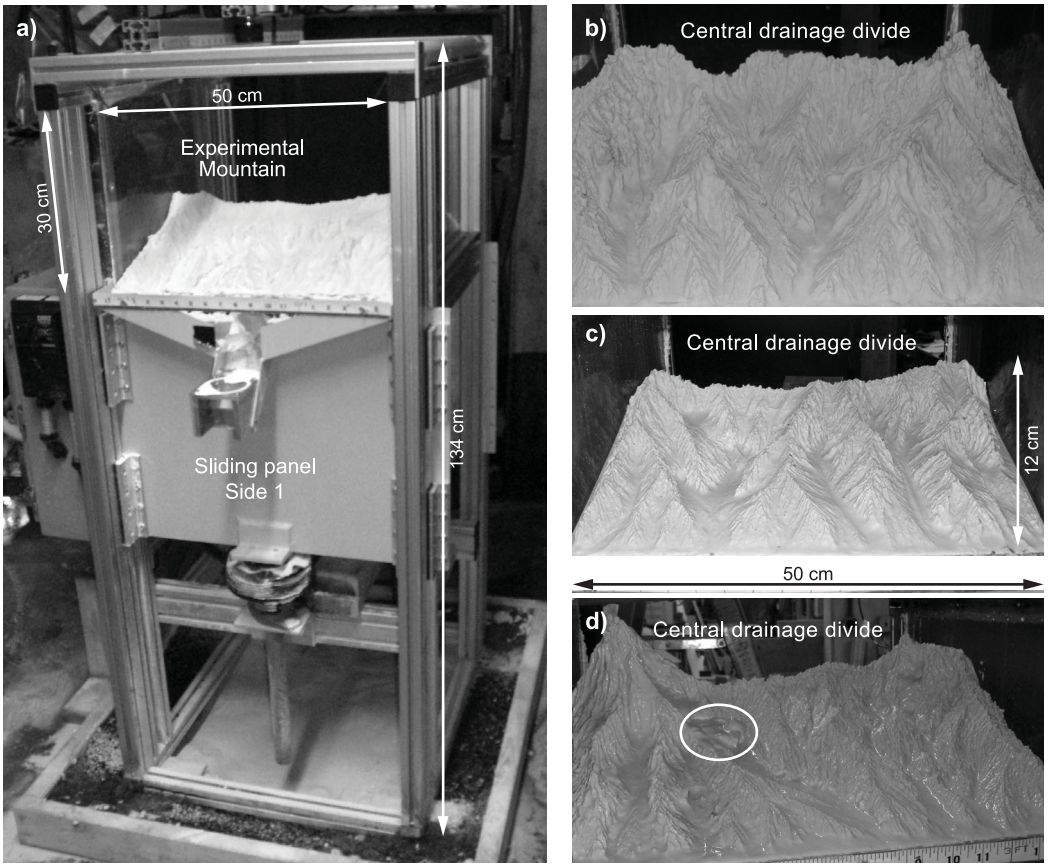

Figure 1. (a) Experimental apparatus (without sediment discharge units) and (b–d) a selection of typical model topographies: note that each photo shows only one side of the model. The internal dimensions of the erosion box are 50 × 50 cm × 30 cm high. At the beginning of each experiment, this box is filled with a paste formed from pure crushed quartz and water, similar to the procedure described by *Hasbargen and Paola* [2003]. A large landslide is highlighted by a white circle in Figure 1d.

There is a general consensus that these physical models have a qualitative relevance from which first-order behaviors can be learned about the real world [*Hasbargen and Paola*, 2000, 2003; *Lague et al*., 2003; *Bonnet and Crave*, 2003, 2006; *Bonnet*, 2009; *Paola et al*., 2009]. The "climate" of each experiment was controlled through the *water-to-rock-ratio* = (precipitation rate × ρ_w)/(U × substrate density [1.9 g cm^{-3}]) [per *Hasbargen and Paola*, 2000, 2003]. This ratio is a qualitative measure of the erosive efficiency of a given precipitation rate relative to surface uplift, i.e., the model "climate" (see Table 1). In our experiments, we controlled the climate ratio by altering uplift rate (Table 1). We effectively model three distinct macroclimates covering water-to-rock-ratios ranging from 0.5 to 0.9 (@ U = 60 mm h^{-1}), 1.0 to 1.8 (@ U = 30 mm h^{-1}), and 3.5 to 5.9 (@ U = 9 mm h^{-1}) with the fourth experiment overlapping these ranges (0.8–1.4 @ U = 40 mm h^{-1}); there also exists a range of smaller-scale microclimates within each model mountain (Figure A1), the potential influence of these microclimates is discussed in detail in Appendix A. A low water-to-rock-ratio corresponds to a relatively dry climate and vice versa. Generating different topographies with differing uplift rates and climates enabled us to draw comparisons between the internal dynamics of different landscapes. Crucially, we make the assumption that if the same behavior is observed in all three macroclimates that behavior arose through internal (autogenic)

Table 1. Parameters Used in All Four Experiments; Potential Sources of Variability in These External Forcing Parameters Are Discussed in Detail in Appendix A[a]

Uplift Rate (mm h^{-1})	Precipitation Rate (Spatial Stdev) (mm h^{-1})	Climate Range
9	71 (13)	3.5–5.9
30	75 (17)	1.0–1.8
40	78 (15)	0.8–1.4
60	78 (15)	0.5–0.9

[a]The standard deviation of precipitation was measured by collecting water in nine pans in a 3 × 3 grid at the base of the apparatus before each experimental run. The climate range refers to the range of water-to-rock-ratios present in each experiment as described above and shown in Figure A1.

dynamics rather than external climatic or tectonic influence.

2.1. Data Analysis

Catchment analysis allowed us to identify the crest of every ridge in every topographic DEM. The local relief of a ridge pixel is calculated as the mean elevation difference between each 1 mm pixel defining the top of a ridge and its adjacent third-order or higher channels (these channels represent the floor of major valleys). To achieve this, a triangular irregular network (TIN) was constructed to create a surface joining these channels. The elevation difference between each ridge pixel and the underlying TIN surface is the local relief. We then calculated the rate of lateral ridge mobility of every ridge cell between each topographic scan; lateral ridge movements $<$1.5 mm or $>$27 mm were discounted from further analysis because (a) in the former case this is the limit of measurement resolution when using 1 mm pixels and euclidian distance estimation; and (b) error analysis outlined in Appendix A suggests that lateral measured movements $>$27 mm are unreliable.

We analyze our results in the context of a SOC system that is characterized by spatial and temporal power law scaling. *Murray* [2007] and *Passalacqua et al*. [2006] have termed this the turbulence paradigm by which the same patterns and processes operate over a wide (but finite) range of scales, giving rise to power law scaling signatures (self-similarity, anisotropic self-affinity, fractals, and multifractals). This type of scaling does not in and of itself mean that SOC behavior is present but its absence does require that SOC is absent [*Phillips*, 1999; *Coulthard and Van de Wiel*; 2007]. As discussed in section 1, to infer SOC as well as identifying power law frequency-magnitude relationships we also identify the mechanism for a "chain of failures" to propagate across a wide range of scales (i.e., a small perturbation can trigger a cascade of responses). We also investigate another key characteristic of SOC systems: f^{-1} power spectra of events (such as river avulsions and landslides) occurring over all time scales, where power is inversely proportional to frequency [*Bak et al*., 1987; *Baas*, 2002; *Malamud et al*., 2004; *Jerolmack and Paola*, 2007].

3. Results

3.1. Description of Model Runs

The slow downward movement of two opposing weirs simulates tectonic uplift, which exposes the silica substrate to erosion (Figure 1). At the beginning of each experiment multiple channels develop along the two weirs: drainage networks then form as channels propagate in toward the center, side branches form simultaneously with the main stem as observed in numerous previous studies of this type [*Parker*, 1977; *Rodriguez-Iturbe and Rinaldo*, 1997; *Hancock and Willgoose*, 2001; *Pelletier*, 2003; *Lague et al*., 2003]. A sediment-water mixture debouches through the weirs where it is weighed. The emergence of multiple drainage networks leads to a rapid increase in sediment discharge and topographic relief (Figure 2). In the three lower uplift rate experiments, sediment discharge generally shows a relatively smooth transition to a stable value (which we show later to be equal to the flux steady state). In the $U = 9$ mm h^{-1} and the $U = 40$ mm h^{-1} experiments, this transition occurs prior to the development of either a central divide or a stable maximum relief. Sediment discharge during $U = 30$ mm h^{-1} did not stabilize until after the formation of a central divide (Figure 2). Sediment discharge during the relatively rapid uplift rate experiment ($U = 60$ mm h^{-1}) showed similar variability to $U = 30$ mm h^{-1} prior to the formation of a central divide, but in contrast to other experiments sediment discharge maintains long-period variability over a large fraction of a relief depth of erosion (Figure 2). We characterize the collective behavior of sediment discharge and topographic relief as growth, transitional, and stable phases, noting that not all experiments show each phase clearly (Figure 2).

3.2. Emergence of Self-Organization

Spatial organization is characterized by the rapid development of fully connected drainage networks with a stable number of large catchments (Figures 2 and 3). Model topography shows two distinct scaling regimes reflecting a difference in process dominance, i.e., between hillslopes $<$100 mm^2 and channels at larger areas (Figure 4). The "average" spatial character of these systems is similar despite initial differences in initial topography, uplift rate, and climate. Drainage networks have a Horton bifurcation ratio of $\sim$3.5, well within the range of 3–5 seen in nature [*Horton*, 1945; *Rodriguez-Iturbe and Rinaldo*, 1997]. Similarly, catchment geometries in all four experiments develop an outlet-spacing ratio ranging between 1.6 and 3.1 with an average

value of 2.16 (Figures 3 and 5) well within the range observed in the field (1.91–2.23, *Hovius* [1996] and 1.41–4.06, *Talling et al*. [1997]) and consistent with numerical modeling results [*Perron et al*., 2008].

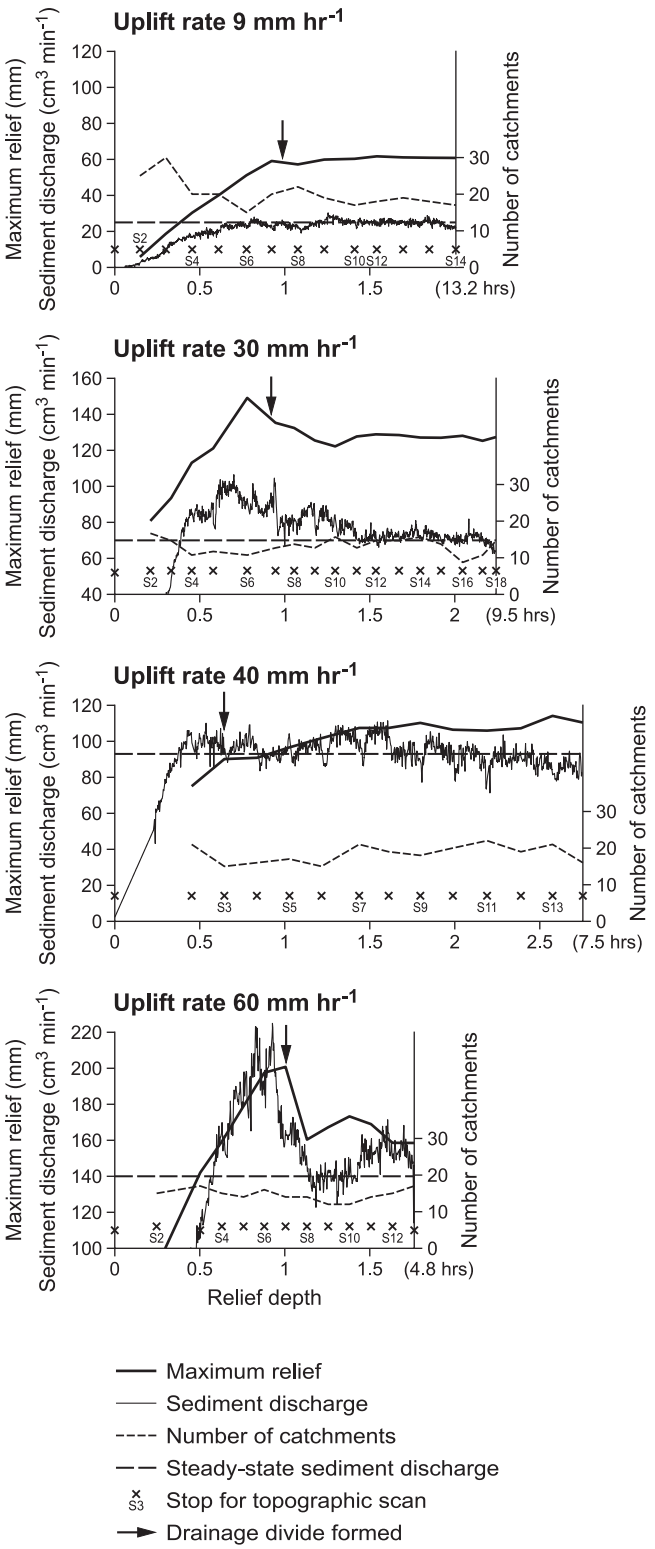

Figure 2.

Both ridges and channels remain highly dynamic throughout each experiment despite the apparent stability of macrotopographic and sediment discharge characteristics (Figure 2). Channel migration is driven by a variety of mechanisms, including internal reorganization due to river capture events, knickpoint migration, and avulsions: each of these processes is sensitive to critical thresholds [*Gardner*, 1983; *Bishop*, 1995; *Whipple*, 2004; *Jerolmack and Paola*, 2007]. The temporal resolution of topographic scans is insufficient to capture alluvial channel dynamics but we suggest that erosion and accumulation of ridge mass (via uplift) is sufficient to dominate over any smaller-scale alluvial signature [cf. *Coulthard and Van de Wiel*, 2007]. Ridges grow as mass is added through uplift or diminish through erosion. We quantified the mobility of ridges using the probability distribution of lateral ridge mobility (Figure 6). In all cases, mobility is well defined by power law trends across a wide (but finite) range of magnitudes. All four experiments show multiscaling, with exponents ranging between 0.7 and 2, implying different process regimes at large and small rates of ridge movement.

Perron et al. [2008] theorized that catchment dynamics are driven by a competition for drainage area (reflecting the ability to capture precipitation), and that this competition leads to the elimination of small catchments as larger catchments outcompete them. The success of this competition is visible in our experiments; in one instance a catchment formed that spanned nearly the entire width of the model mountain (Figure 5, scan 7). Logically once a very large catchment "beats" its neighbors in this manner it should consistently outcompete them and remain relatively large. But this is not what we observe: very large catchments tend to shrink or split into smaller units (Figure 5). Thus, expansion of a catchment beyond a certain size appears to be unstable and by

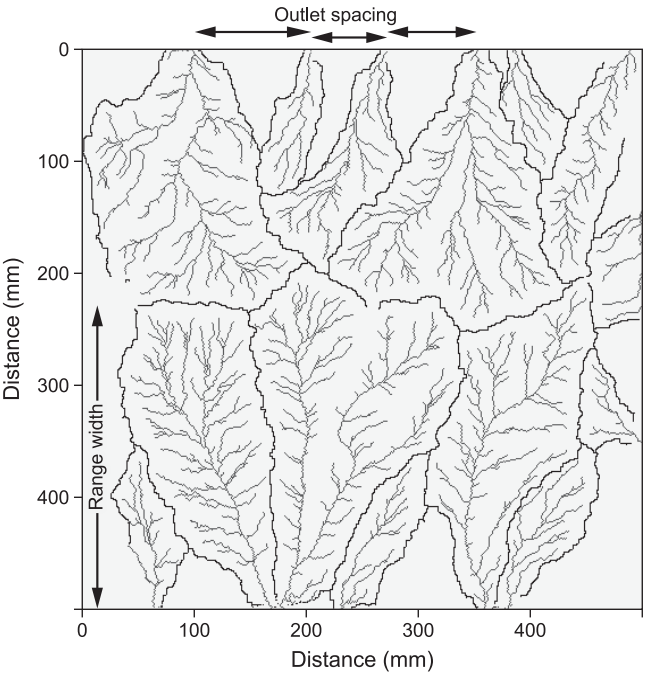

Figure 3. Typical drainage and ridge network configuration: dark black lines are ridges, gray lines are the channels. The outlet-spacing ratio referred to in text is defined as the range width divided by the outlet-spacing along a range front as shown here [*Hovius*, 1996]. Note that only major drainage basin occupying >1% of surface area is shown and used in data analysis (e.g., Figure 2). The flow accumulation threshold for initiation of channels is 100 pixels in agreement with hillslope-channel scaling shown in Figure 4.

the end of each experiment large catchments hold roughly similar geometries (Figure 5). In later discussion, we will argue that this stable catchment geometry is a function of SOC.

The emergence of self-organization is accompanied by fluctuations in sediment discharge. Discharge flowing from each side of the model represents the combined output from three or more catchments making it impossible to identify individual storage-and-release events (topographic laser scans are too infrequent to capture discharge dynamics at any useful resolution). Instead, we look to the overall scaling of sediment discharge, which in this instance is characteristic of SOC (Figure 7). All of the experiments exhibit $\sim f^{-1}$ scaling in their power spectra, regardless of uplift rate and climate (Figure 7) [*Bak et al*., 1987; *Bak*, 1996]. In essence, this scaling indicates that internal system dynamics, regardless of external stimuli, are generating "events" at all magnitudes with small events the most common and vice versa.

3.3. Emergence of a Threshold-Related Hierarchy in Catchment Dynamics

It is notable that all ridges are equally mobile during the early stage of each experiment (Figure 8). Ridges begin to self-organize after ~1 relief depth of erosion; at this stage lateral mobility of small-ridges is dependent on local-relief, while large ridges develop a complex scaling that is far less sensitive to relief (Figure 8). Interestingly it is over this same "time scale" that spatially uniform erosion (or a dynamic equilibrium) is observed in the experiments of *Hasbargen and Paola* [2003]. By ~1.8 relief depths of erosion, a clear threshold has emerged separating two distinct scaling regimes. This threshold is centered about a relief index of 0.3 ± 0.1 regardless of uplift rate or climate. In absolute terms, the location of the threshold lies between 9 and 26 mm local relief depending on the experiment (Figure 8). A coherent pattern is also observed for the scaling threshold in terms of lateral mobility index (Figure 8) with most values lying at 0.2 (corresponding to 2–12 mm h^{-1} depending on the experiment). Similar scaling thresholds are also seen in the probability distribution functions of lateral mobility (Figure 6) where we observe a reduction in log linear slope (to 0.7) at small scales.

Figure 2. Maximum relief, total sediment discharge from both sides of each experiment, and the number of large catchments in all four experiments. Maximum relief is the maximum elevation of the central drainage divide during each scan. To enable intercomparison between models with differing rates of uplift, the *x* axis is cited in relief depths ((model run time × uplift rate)/mean elevation of the central drainage divides during the last five topographic scans from each experiment) [cf. *Hasbargen and Paola*, 2000, 2003]. This mean elevation corresponds to one "relief depth" of the model mountains which @ $U = 9$ mm $h^{-1} = 61$ mm, @ $U = 30$ mm $h^{-1} = 127$ mm, @ $U = 40$ mm $h^{-1} = 109$ mm, @ $U = 60$ mm $h^{-1} = 165$ mm. The point in each experiment when the central drainage divide fully forms is shown by downward pointing black arrows. The value of sediment discharge at flux steady state (when mass influx = sediment + groundwater discharge) is indicated by a dotted horizontal line in each graph. Steady sediment discharge (Q_{ss}) is backed out from the sediment/water ratio ($\mu = 0.56$) of the eroding substrate after a flux steady state is established: where $Q_{ss} = U.A.\mu$, U = uplift rate, A is the model area. We make the assumption that μ in the slowest experiment ($U = 9$ mm h^{-1}) is representative of all four experiments; this is reasonable given that the same mixing procedure was followed in each case. In addition the "time" of every topographic scan is shown: note that each scan is accompanied by a very short-term perturbation in discharge due to the need to turn precipitation off during each laser scan.

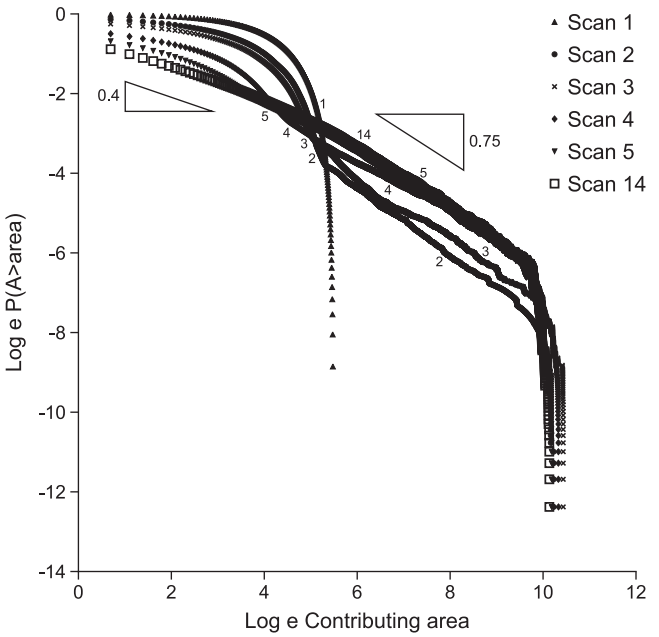

Figure 4. Cumulative distribution of drainage area of all pixels in sequential DEMs taken from the $U = 9$ mm h^{-1} experiment on natural log axes; the other experiments are consistent with this pattern. Lines numbered 1–5 and 14 are the topographic scan IDs corresponding to the scan numbers shown in Figure 2. There is little change in drainage area structure beyond scan 5. Slope angle (σ) is denoted by the two triangles. Statistical scaling takes the probabilistic form of $P(A \geq \text{area}) \propto \text{area}^{-\sigma}$, which describes the self-similar character of the relative occurrence of drainage areas. Drainage area distributions rapidly converge toward a stable log linear distribution after ~0.5 relief depths of erosion (between scans 4 and 5: Figure 2). This reflects the development of a fully connected drainage network as channels rapidly incise headward into an initially flat surface. We observe two distinct power law forms in the final distribution; at areas $\sim<100$ mm^2 the slope (σ) is 0.4 which then increases to 0.75, at larger areas, finite size effects due to the boundaries of the experimental apparatus drastically reduce the number of observations. These two scalings reflect the transition from slope-dependent hillslope processes at small areas to threshold limited drainage channels at larger areas [*Rodriguez-Iturbe and Rinaldo*, 1997].

The effect of the self-organization of ridges into two distinct scaling regimes is illustrated spatially in Figure 9. When the locations of all ridges through time are overlain together it is clear that the shape, size, and location of major catchments vary through time. However, when small ridges at or below the (model specific) scaling threshold are excluded a stable ridge configuration emerges (Figure 9, right): this effect is particularly evident in the 40 mm h^{-1} experiment. It is important to note that the highly mobile small relief ridges are seen all the way back to the central drainage divide; conversely in the 40 mm h^{-1} experiment, large ridges can be seen to extend to the mountain front. Thus, small and large ridges, and their attendant dynamics, are observed throughout the model mountains and no particular behavior appears to be limited to model boundaries. This suggests that our strategy of cropping each DEM 10 mm inward from the weirs prior to analysis effectively negates the influence of this model boundary. Overall, it is clear that the small highly dynamic ridges are masking a larger-scale order (Figure 9, right). In this emergent order, the perpetual dynamism of large ridges is expressed not as constant reorganization of catchments but instead as minor oscillations about a stable mean location.

4. Discussion

Hasbargen [2003] argued on the basis of purely geometric considerations that small ridges should be more mobile than large ridges and this seems intuitively reasonable. However, ridge geometry cannot explain the observed emergence of two clear scaling regimes in ridge dynamics. Instead, the emergence of a hierarchy in scaling behaviors is suggestive of a complex system in which each emergent component acts to limit the degrees of freedom of the process that created it [cf. *Werner*, 1995, 1999]: once stable catchments emerge, they appear to limit the degree of freedom of the large ridges from which they are formed, i.e., large ridges are highly dynamic early on in the experiment but once a stable basin geometry emerges (Figure 9) their dynamism becomes restricted by the catchment geometry. Moreover, perhaps counterintuitively, the very largest ridges are no more or less stable than medium sized ridges; evidently only the smallest ridges retain their dynamism throughout the lifetime of each model mountain. This behavior is similar in all climates modeled here suggesting that it is a robust indicator of how high-relief catchments behave in the real world.

It is useful to examine the scaling relations observed here in the context of a flux steady state (in which tectonic influx = erosional efflux): that is, is flux steady state a requirement for the emergence of landscape scaling as described above? We described earlier (section 3.1) three stages of model landscape development: growth, transitional, and stable. In order to place these developmental stages into a meaningful

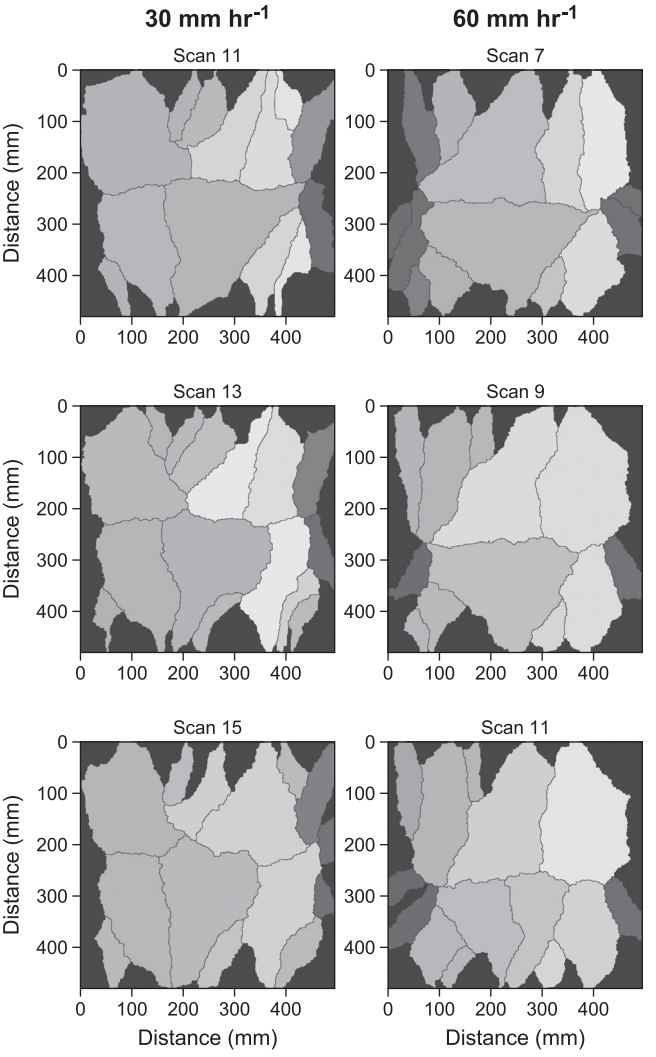

Figure 5. Typical sequences of changing catchment geometries taken from the 30 and 60 mm h^{-1} experiments. These images were selected to highlight that very large catchments do occasionally form but these inevitably shrink and divide into smaller forms. By the end of each experiment, a stable catchment geometry has emerged. Scan numbers correspond to the times shown in Figure 2.

context, we calculated the sediment discharge steady state values for each experiment (Figure 2). We note that the onset of flux steady state does not correspond simply with either topographic steady state or the time at which the central divide forms. And in the case of the fastest experiment, the appearance of flux steady state is relatively brief, between ~1.2 and 1.4 relief depths. Inspection of Figure 2 suggests that the emergence of the two distinct scaling regimes seen in Figure 8 more closely corresponds to the time of formation of the central divide and the *emergence* of stable catchment geometries (Figure 9, right) rather than to the establishment of a flux steady state.

We here argue that our models exhibit complex *SOC* behavior both in time and space. The probability distribution function of ridge movement exhibits power law scaling (Figure 6), in this instance multifractal as two scaling regimes emerge in catchment ridge dynamics (Figure 6), indicative of an SOC system [*Sapozhnikov and Foufoula-Georgiou*, 1996; *Coulthard and Van de Wiel*, 2007]. Moreover, sediment discharge exhibits $\sim f^{-1}$ spectral scaling across a wide range of frequencies (Figure 7). Such scaling is consistent with the *Bak et al.* [1987] sand pile model for SOC behavior and implies that a critical process dominates sediment discharge [*Coulthard and Van de Wiel*, 2007]. The critical process driving ridge migration appears to be landsliding, driven in a fundamental sense by the competition between catchments for discharge [cf. *Perron et al.*, 2008] but in terms of process probably via lateral channel migration undercutting ridges and knickpoint propagation; both processes are observed in all experiments. Certainly our observation during model runs and the $\sim f^{-1}$ spectral scaling of sediment discharge suggests that landsliding is the critical process [*Bak et al.*, 1987] but the role played by knickpoint migration is ambiguous. Channel incision by itself should only release a relatively small mass compared to the movement/destruction of a major ridge, but we know from our own qualitative observations and from *Hasbargen and Paola* [2003] and *Bigi et al.* [2006] that knickpoints also tend to destabilize adjacent slopes and cause landslides. Thus, whatever the trigger, it is clear that landslides are the result; we do not suggest that landslides are the only slope process driving erosion, merely that it is the most effective at driving ridge migration. For instance, we know from field observations that landslides exert a first-order control on catchment structure through "*catastrophic divide shifting*" [*Korup et al.*, 2010]. As a landslide pushes a ridge laterally the failed slope will lower in angle while in the adjacent catchment the ridge slope will either steepen if the landslide moved the ridge in that direction or remain at its current (steep) angle. This slope asymmetry will produce relatively high erosion on the steeper slope either through slope-dependent erosive process(es) or more likely landsliding and thus the observed "push back" of the ridge from whence it came (Figure 9): this is the same mechanism identified by *Hasbargen and*

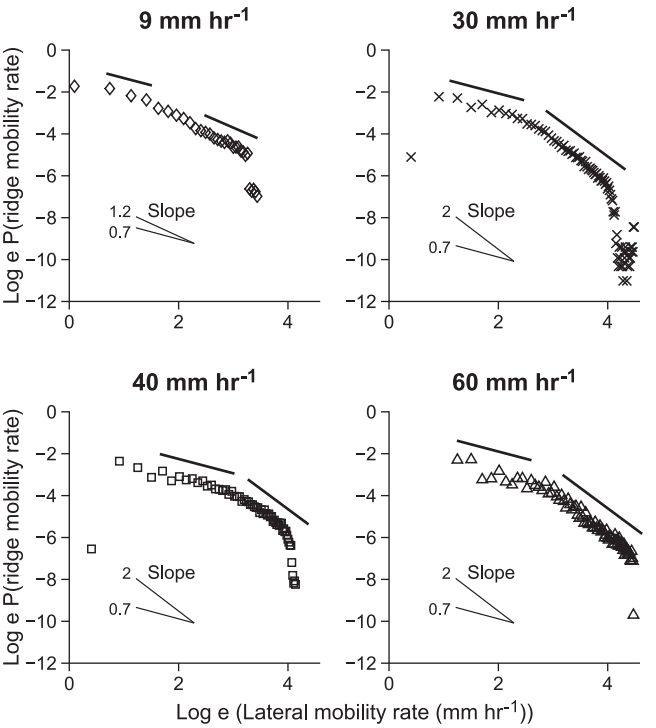

Figure 6. PDF of lateral ridge mobility of all ridge pixels in all topographic scans from each experiment after the formation of a central drainage divide on natural log axes. The probability density scaling takes the form of $f(x) \propto x^{-(\sigma+1)}$ which describes the self-similar character of fluctuations in ridge mobility. Finite scale effects related to the maximum size of individual catchments are observed at the largest rates of mobility.

Paola [2003] to explain ridge oscillations in their experiments, and it has been called on to explain the first-order shape of thrust-fault derived mountain ranges [*Ellis and Densmore*, 2006]. Occasionally, a ridge failure may be so significant that it leads to the destruction of the ridge (or moving it a great distance before stabilizing) and capture of an adjacent catchment hence the development of extralarge catchments (Figure 5). The successful expansion and later destruction of large catchments (Figure 5) will produce large pulses of discharge as sediment is "stored" in ridges (as they accumulate mass during uplift) and released during ridge movement. Crucially these small and large ridge movements provide a mechanism for a "chain of failures" across all scales, one of the primary attributes of a SOC system [*Coulthard and Van de Wiel*, 2007].

An SOC system maintains a *resilient* quasi steady critical state around which it self-organizes [*Coulthard and Van de Wiel*, 2007; *Keiler*, 2011]. In our experiments, a fully connected drainage network quickly develops (Figure 4), thereafter the number of catchments remains stable (Figure 2) and catchment geometries converge toward stable configurations (Figure 9). This large-scale order is often masked by smaller-scale topographic dynamics (Figure 9). These results are consistent with the perpetual ridge dynamics of *Hasbargen and Paola* [2000] and *Goren et al*. [2014] while also showing how stable topography may arise at large length scales. This result was anticipated by *Phillips* [1999] who argued that chaotic elements can exist at some small scales while order may emerge at the largest scale; importantly our results differ insofar as in our models stable catchments are smaller than the largest possible size (Figure 9). We observed in section 3.2 that even when major ridge excursions occur and form very large catchments these are unstable and tend to shrink back to the quasi-stable geometry that emerges after ~1 relief depth of erosion (Figures 5 and 9), thereby implying an intrinsic resilience in these systems. It seems logical to propose that this resilience arises from a critical balance reached as catchment bounding ridges push back and forth (and are occasionally created or destroyed) until a stable configuration is "found," i.e., the stable outlet-spacing observed in our experiments (Figure 9) and in field and numerical modeling studies [*Hovius*, 1996; *Talling et al*., 1997; *Perron et al*., 2008]. It follows that the critical state is not dependent upon the maximum size of the system but rather by the interplay between advective erosion processes (such as channel incision) and diffusion-like mass transport, as predicted numerically by *Perron et al*. [2008].

We argued in section 2 that if the same behavior is observed in all four experiments with three distinct macroclimates, then it is reasonable to conclude that behavior arose through autogenic dynamics rather than external forcing. Potential causes of variability in external forcing, namely uplift rate and precipitation are discussed in detail in Appendix A; we conclude that the rate of base-level lowering is constant and that the modeled landscapes are insensitive to observed spatial and temporal variability in the pattern of precipitation. Instead, the consistent spatial and temporal power law scaling observed in three climatically distinct experiments argues for a landscape dominated by internal system dynamics. Our experiments seem to further suggest that that it is SOC topographic dynamics that generate stable catchment geometries and thus lead to the emergence of the observed complex system but we

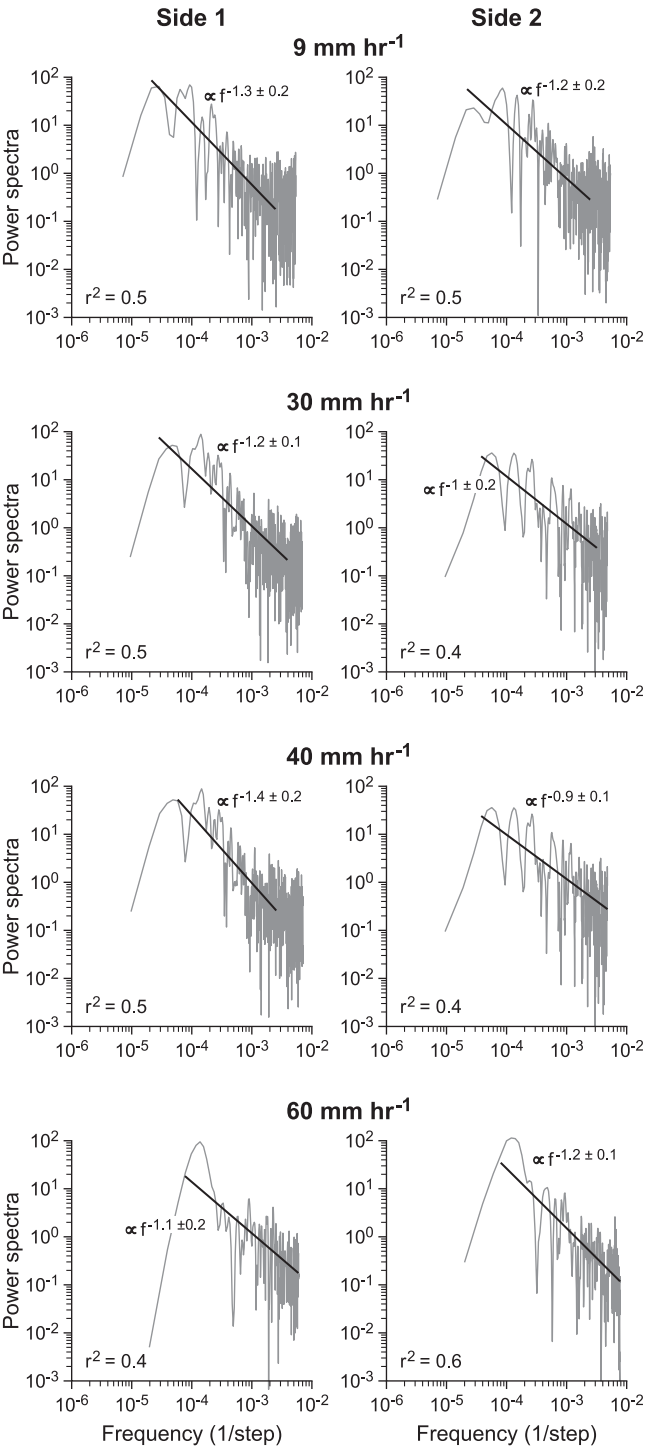

Figure 7. SOC scaling of sediment discharge on each side during all four model runs. In all cases, discharge follow power law scaling, within the range defined by the fit lines, at or very close to f^{-1} scaling [cf. *Bak et al.*, 1987]. The 95% confidence intervals of the power law scaling exponents are shown. Best fit lines were fitted in matlab using robust bisquare log linear regression and the r^2 good-of-fit shown [*Huber*, 1981]. Lomb-Scargle spectral analysis of unevenly spaced data was used because the time step between discharge measurements varied between 30 and 45 s depending upon discharge rate. The first 0.5 relief depths of erosion in each model run are not included in this analysis.

acknowledge that the "chicken and egg" of this issue cannot be fully resolved from our data. What we can state is that once an SOC landscape forms it does not evolve; its statistical properties become stationary, even though large fluctuations can and indeed must occur [*Bak et al.*, 1987; *Bak*, 1996; *Sapozhnikov and Foufoula-Georgiou*, 1996]. In such landscapes, minor external perturbations should rapidly disappear into a melee of large-scale competing negative (e.g., ridge push back and forth) and positive internal feedbacks (e.g., the capture of discharge driving catchment expansion), while very large-scale external forcings (perhaps analogous to glacial-interglacial cycles) only produce fluctuations about the critical state.

5. Conclusions

Internally generated SOC processes create complex, critically balanced mountain landscapes that operate in a similar fashion regardless of rates of tectonic uplift or climate. In all four experiments, a fully connected drainage network emerges by 0.5 relief depths of erosion while a twofold hierarchy of catchment bounding ridges begins to emerge after ~1 relief depths of erosion; this hierarchy fully develops at ~1.8 relief depths of erosion (Figure 8). By this stage, a clear threshold has emerged separating two distinct scaling regimes; where large ridge mobility is insensitive to relief and small ridge mobility is relief dependent (Figure 8). Spatial and temporal power law scaling is the norm in all four experiments: both in terms of the magnitude and frequency of ridge movement and in the ~f^{-1} spectral scaling of sediment discharge from both sides of each model mountain. This scaling implies not only that a critical process dominates landscape dynamics (i.e., landsliding) but that the same mechanism is responsible for highly dynamic ridge-and-valley topography. The

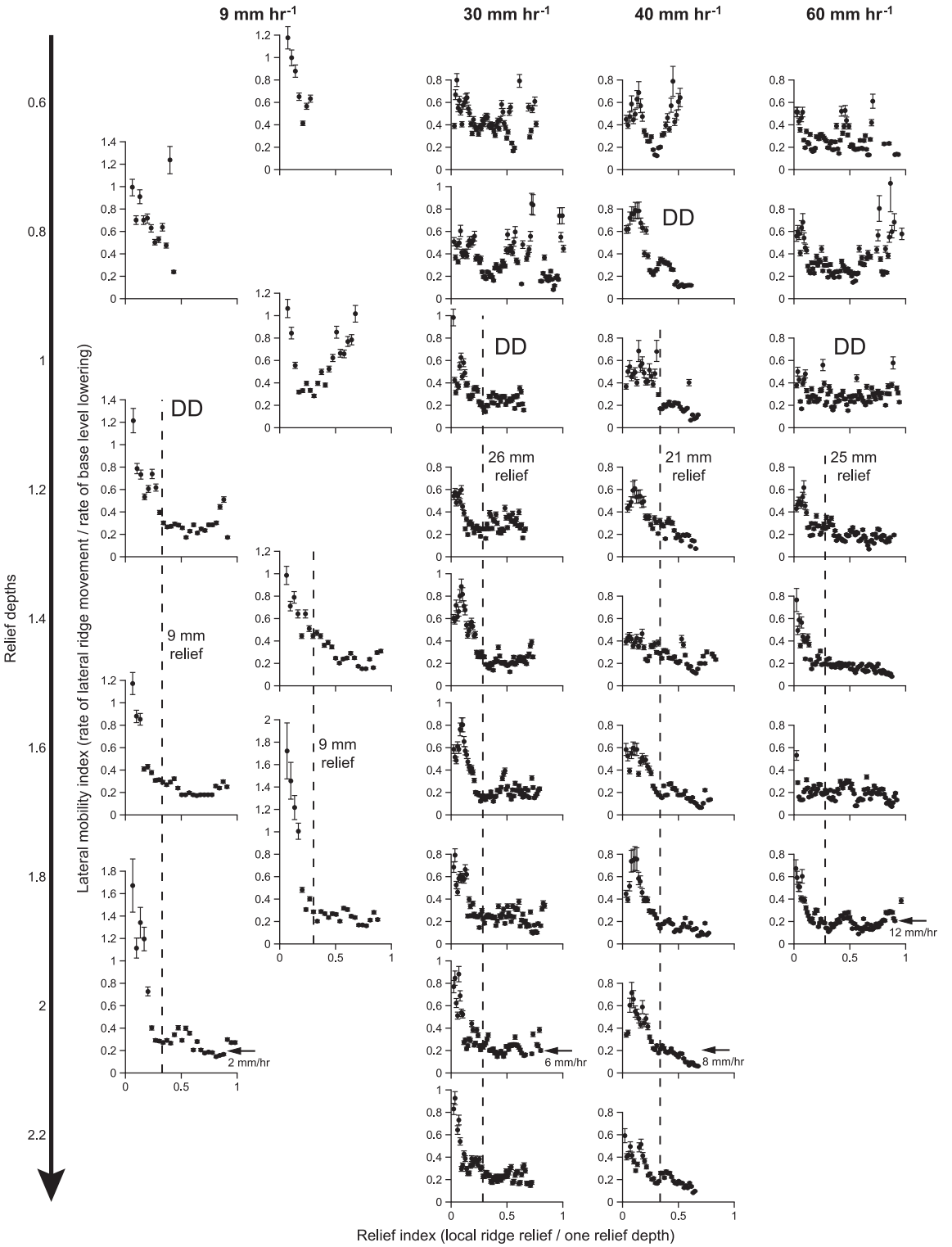

Figure 8. Normalized median rates of lateral ridge mobility as a function of local relief plotted through time from top-to-bottom. DD refers to the point in each experiment when the central drainage divide forms. Relief depth is defined in Figure 2. As the experiments progress, ridge mobility becomes insensitive to ridge relief beyond a threshold value (denoted by dotted vertical lines: actual relief shown). The mobility of large ridges exhibits occasional deviations from a simple linear relationship throughout these experiments reflecting major movements of catchment boundaries and/or the central diving ridge, e.g., the lowermost figure in the right-hand column. Local relief (elevation difference between ridge crest and adjacent valley floor: see section 2) is normalized against one relief depth. Lateral mobility rates are binned into 1 mm relief bins and the median value plotted here: the absolute mobility rate at the threshold value near the end of each experiment is shown with sideways pointing arrows. The 95% percentile error of median mobility rates is shown here (see Appendix A for explanation and Figure A2). We here ignore median ridge movements >27 mm between scans (see Appendix A); such large movements are very rare occurring <1% of the time.

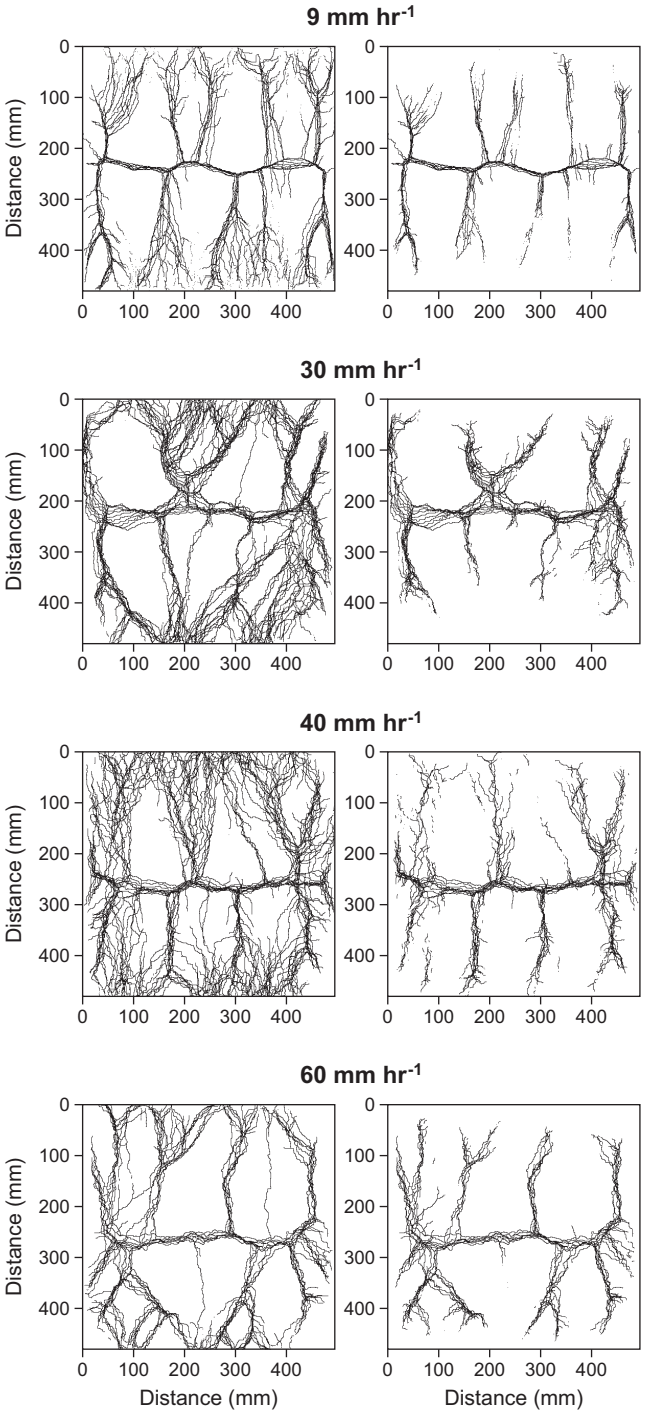

Figure 9. (left) Pattern of movement of all ridge-top pixels during each experiment and (right) only those ridge-top pixels that exceed the threshold of relief: @ 9 mm h^{-1} = 9 mm; @ 30 mm h^{-1} = 26 mm; @ 40 mm h^{-1} = 21 mm; @ 60 mm h^{-1} = 25 mm. These data are compiled from all topographic scans after 1 relief depths of erosion has occurred (see Figure 8).

larger ridges form the boundaries of regularly spaced catchments, with an average outlet-spacing ratio of 2.16. Once formed, large catchment bounding ridges oscillate about a critically balanced mean location as mass movement pushes ridges back and forth. Smaller ridges remain highly dynamic as they constantly form and reform smaller-scale topography. These scalings and behaviors are similar despite a wide range of uplift rates (9, 30, 40, and 60 mm h^{-1}) and macroclimates and microclimates. Stable catchment topography arises independently of external (climatic) forcing and is instead dependent upon the interplay between autogenic channel dynamics and hillslope processes.

The emergence of a complex landscape, with a hierarchy of ridge dynamics dominated by SOC behavior, creates a resilient topography unlikely to be sensitive to external perturbations. This is perhaps counterintuitive as a key characteristic of SOC systems is that small perturbations can cause changes across all scales and we do observe major changes in catchment structure during our experiments. Occasionally, the competition for discharge drives a cascade of ridge failures and the expansion of a single catchment at the cost of its neighbors. These expanding catchments never reach the maximum possible size dictated by model boundaries; instead even when an extralarge catchment forms it shrinks until it attains a stable geometry, implying a high degree of resilience to these systems. We also observe this intrinsic stability at larger scales in terms of a near-constant number, size, and spacing of catchments. As well as informing these arguments our experiments also demonstrate that the development of dynamically stable large-scale landforms is related to the emergence of a complex-system hierarchy in topographic dynamics. Once formed, these landscapes do not evolve in any "direction"; statistical properties such as average topography and discharge become stationary while at a smaller-scale catchment bounding ridges dynamically oscillate about a mean catchment geometry.

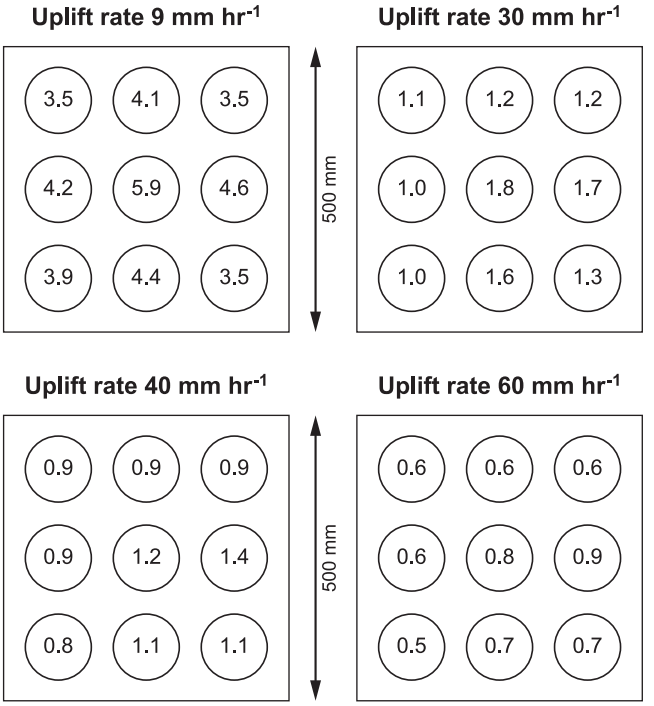

Figure A1. The spatial pattern of "climate" at the base of the erosion box as defined by the water-to-rock-ratio (see section 2): high values correspond to a relatively wet climate and vice versa. The values cited here derive from rainfall into a uniform array of measuring cups prior to the experiments and averaged over 75–104 min depending on the experiment.

Appendix A: Uncertainty Analysis

A1. Sources of Temporal and Spatial Variation

Our experimental design depends on the assumption that sources of topographic and discharge variability are internal rather than external; specifically that there is no significant variation in the rate of tectonic uplift (i.e., simulated by weir lowering) or precipitation during the course of each experiment. We here assess potential sources of variability in these two parameters.

A1.1. Temporal Variability

There are two potential sources of temporal variability in our experimental setup: (1) the rate of weir lowering on either side of the experiment; and (2) temporal variation in the rate of precipitation experienced by the eroding surface. In the former case, we used the topographic laser scanner to measure downward movement of each weir every 30–60 s depending on the experiment. In all cases, we observe regular downward movement within the <1 mm resolution of the scanner; on a few rare occasions a small ($\sim$1 mm) jog in weir movement is observed immediately after stopping for a topographic scan. Even allowing for these minor disturbances when time versus weir movement is plotted, in all experiments a regression line fits the time series with an $r^2 = 1$.

Externally controlled variation in total precipitation has two potential sources: (A) In our experimental design, we periodically turned off precipitation for 9 or 10 s to take overhead photographs at time intervals of 360s (@ $U = 9$ mm h^{-1} and $U = 30$ mm h^{-1}), 180 s (@ $U = 40$ mm h^{-1}) and 300 s (@ $U = 60$ mm h^{-1}). In addition precipitation was turned off for $\sim$20 min during each topographic laser scan. While the effect of periodic dry spells cannot be completely discounted we can deduce no link between these short periodic perturbations and the scaling behavior of ridges nor in the emergence of a regular catchment structure; (B) Uncontrolled variation in precipitation from the overhead rainfall simulator might produce variable discharge. A steady inflow of water through the rainmaker was ensured through the use of a pressure valve controlled pump that extracted water from a reservoir rather than the mains water supply. We sought to characterize the temporal stability of precipitation and resulting discharge. Discharge is a time-varying mixture of water from precipitation, interstitial water from the eroding substrate and eroding sediment. Water discharge can be calculated from this admixture using a variation of equation (1) but in our dischargeometer measurements (time taken to fill a fixed volume) water and sediment discharge is perfectly correlated. Thus, water discharge measurements are dependent on variability in erosion. We minimized the importance of variable erosion by extracting a steady state water-sediment discharge record (between scans 10 and 13 and excluding the effect of the controlled pauses in A above) from the 9 mm h^{-1} experiment; in this record sediment discharge accounts for $\sim$10% of total discharge. We found that the coefficient of variation in discharge (Stdev/mean) over this period never exceeds 0.03 regardless of the time period over which it is calculated; we followed a moving window approach to calculate the coeff-var over time increments ranging from minutes to >1 h. Given identical rainfall simulator design elements between experiments it follows that temporal variation in water discharge is negligible throughout our model runs.

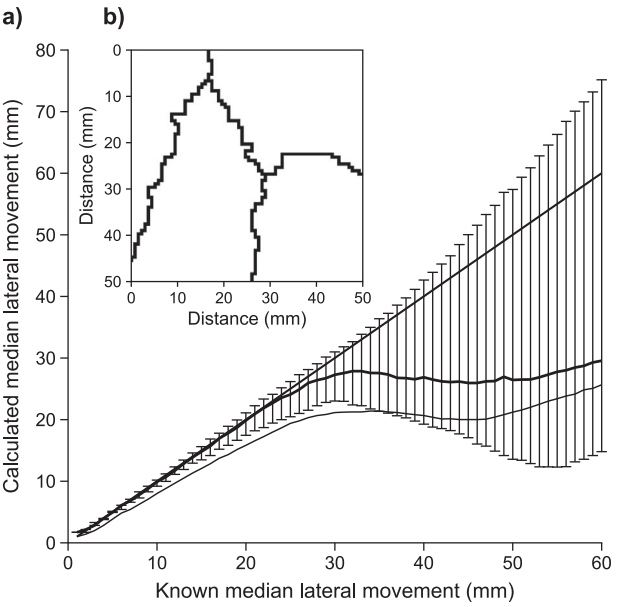

Figure A2. Estimating the error and bias in measuring the median rate of lateral ridge movement. The known median rate of lateral mobility is here compared with the estimated median quasi-Euclidian distance in a typical model. (a) The dotted line shows the initial biased estimate, the thick curved line above is the median line after systematic bias has been removed. The straight black line is the 1:1 line between both variables: deviations from this line indicate a systematic bias in estimating median movement. Error bars are 95th percentiles of distribution from 1000 iterations after bias removal. The relationship between known and calculated movement breaks down at ~27 mm. This threshold distance appears to be related to valley width; as ridges move beyond 27 mm they begin to approach ridges that had been on the opposite side of the valley in the previous topographic scan. (b) Inset, a typical 50 × 50 mm ridge extract from one iteration.

Overall, we agree with *Paola et al.* [2009] these landscapes are not sensitive to small variations in rainfall be they controlled or uncontrolled.

A1.2. Spatial Variability

Each model mountain is subject to a stable but diverse pattern of precipitation that creates distinct microclimates (Figure A1). Over time scales ≥40 min, differences between repeat measurements of rainfall (at each collection cup: Figure A1) yield a low coefficient of variation of ≤0.04. The presence of stable patterns of precipitation, and thus microclimates, over relatively long time scales is consistent with the temporally stable fluid discharge discussed previously. Conversely, over shorter time scales the spatial pattern of precipitation is highly variable; for example—where data are available—we compared the difference in precipitation between short-term (P_S, 26–33 min) and long-term calibration measurements ($P_L \geq 40$ min) and estimate a coefficient of variation, β ranging from 0.16 to 0.21, where $\beta = \text{stdev}(P_L - P_S)/\text{mean}(P_L)$. We do not have any precipitation data over shorter time scales but assume that spatial variability is even higher when measured over minutes or less. *Lague et al.* [2003] speculated that variable rainfall rather than internal dynamics is the cause of the topographic dynamics observed by *Hasbargen and Paola* [2000] and in their experiments. However, more recent numerical modeling results support *Hasbargen and Paola*'s [2000] argument that internal system dynamics cause the high degree of ridge mobility observed in their experiments [*Goren et al.*, 2014; *Willett et al.*, 2014]. We cannot quantitatively assess how important is the effect of short-term rainfall fluctuations on ridge dynamics, because we would need an experiment with perfectly uniform rainfall to test against, but we do offer the following two observations: (1) despite highly variable short-term precipitation and the presence of persistently "wet" and "dry" areas (Figure A1) the spatial pattern of ridge mobility is uniform in all experiments (Figure 8), i.e., neither small (fast-moving) nor large (slow-moving) ridges are restricted to any particular portion of the landscapes. (2) If spatial variation in precipitation has a significant influence on topography we would expect high topography in drier areas and lower topography in wetter areas [cf. *Bonnet and Crave*, 2003]. At the macroscale, this is exactly what we observe: in our four experiments (from slow uplift to fast, and from wet to dry), mean water-to-rock ratios of 4.2, 1, 1, and 0.7 are associated with mean (95th percentile) mountain elevations of 27(50) mm, 49(96) mm, 53(89) mm, and 62(122) mm, respectively, as predicted by *Bonnet and Crave* [2003]. However, we observe no consistent relationship between microclimate and elevation: in our experiments the mid-right-hand portion of the central drainage divide is persistently "wetter" than the left side (Figure A1) yet in the $U = 30$ and 40 mm h^{-1} experiments this wetter section tends to hold a higher elevation (average = 5 mm); in the other two experiments ($U = 9$ and 60 mm h^{-1}) the left side central divide tends to be higher by anything up to 26 mm in the 60 mm h^{-1} model: these measurements are based on the 95th percentile of ridge elevations on the left-hand versus right-hand third of the drainage divide during the final six scans of each model run. Thus, the spatial pattern of precipitation has little or no relationship with topography and overall we conclude that the regular catchment structures and power law scaling observed in our experiments are in all likelihood a function of internal system dynamics.

A2. Error in Measuring Median Ridge Movement

The rate of lateral ridge movement was estimated as the quasi-Euclidian (Matlab®) distance moved by each ridge pixel divided by the time between each scan (typically 0.5 h). We estimated the error associated with calculating the median rate of movement using a Monte Carlo approach. This method begins by randomly selecting a small 50 mm $\times$ 50 mm section of ridge (Figure A2b) and moving the ridge segments laterally in 1 mm increments. After each 1 mm increment the apparent lateral movement is measured for every pixel and the median apparent movement saved. This enables comparison between actual movement and the median lateral movement (Figure A2a); because of the complicated ridge topography individual movement estimates are unreliable hence our focus on median movement. These steps were iterated 1000 times in three scans taken from all four experimental runs, i.e., 12 scans in total. We found that estimates of apparent lateral movement become unreliable at distances greater than 27 mm, beyond which there is no relationship between known median lateral movement and estimated median movement. We also identified a bias in median estimates whereby median lateral distances were systematically underestimated (Figure A2a). This bias was robust in all four scans and thus amenable to correction. We calibrated a fourth-order Gaussian fit to the data and used this to remove the bias; we achieved this by applying a bias correction to every individual lateral ridge pixel movement calculation and recalculating the median movement. This has the effect of shifting the median toward its true value for all movements $<$27 mm. Finally, the utility of this bias correction was tested on a different set of three topographic scans from each experiment, following the methodology outlined above, with the sole difference being that the bias correction was applied before comparing actual lateral movement (in 1 mm increments) with median apparent movement (Figure A2). The 5th and 95th percentiles of the difference between actual movement and apparent median movements from all test iterations were then taken to represent the confidence interval of median movement estimates. This enabled us to estimate the uncertainty in median mobility *rate* (distance/time between topographic scans) of each 1 mm relief bin by propagating these errors in quadrature (Figure 8).

Acknowledgments

We are grateful to the National Center for Earth Surface Dynamics at St. Anthony Falls Hydraulics Laboratory, University of Minnesota, for the provision of technical facilities. We are grateful to Helen Jones and Maria Wilson for help with the figures and manuscript preparation, respectively, and to Chris Paola for hosting L.R. at SAFL and for the many interesting discussions they had. Thanks to Erich Scholz who designed and built the original experimental apparatus, and to Chris Ellis and Jim Mullen who designed and built the dischargeometers and topographic laser scanning system. We acknowledge the Center for Earthquake Research and Information, University of Memphis, for financial support to L.R. All data relevant to this paper are available from the authors. This paper is published with permission of the Director of the BGS.

References

Ahnert, F. (1970), Functional relationships between denudation, relief and uplift in large mid-latitude drainage basins, *Am. J. Sci.*, *268*, 243-263.

Baas, A. C. W. (2002), Chaos, fractals and self-organization in coastal geomorphology: Simulating dune landscapes in vegetated environments, *Geomorphology*, *48*, 309-328.

Bak, P. (1996), *How Nature Work: The Science of Self-Organized Criticality*, Springer, N. Y.

Bak, P., C. Tang, and K. Wiesenfeld (1987), Self-organized criticality: An explanation of the 1/f noise, *Phys. Rev. Lett.*, *59*, 381-384.

Bigi, A., L. E. Hasbargen, A. Montanari, and C. Paola (2006), Knickpoints and hillslope failures: Interactions in a steady-state experimental landscape, *GSA, Spec. Pap.*, *398*, 295-307, doi:10.1130/2006.2398(18).

Bishop, P. (1995), Drainage rearrangement by river capture, beheading and diversion, *Prog. Phys. Geogr.*, *19*(4), 449-473, doi:10.1177/030913339501900402.

Bonnet, S. (2009), Shrinking and splitting of drainage basins in orogenic landscapes from the migration of the main drainage divide, *Nat. Geosci.*, *2*, 766-771.

Bonnet, S., and A. Crave (2003), Landscape response to climate change: Insights from experimental modeling and implications for tectonic versus climatic uplift of topography, *Geology*, *31*, 123-126.

Bonnet, S., and A. Crave (2006), Macroscale dynamics of experimental landscapes, in *Analogue and Numerical Modelling of Crustal-Scale Processes*, vol. 253, edited by S. J. H. Buiter and G. Schreurs, pp. 327-339, *Geol. Soc. of London, Spec. Publ.*, London, U. K.

Brunsden, D. (1993), The persistence of landforms, *Z. Geomorphol., Suppl.*, *93*, 13-28.

Brunsden, D., and J. B. Thornes (1979), Landscape sensitivity and change, *Trans. Inst. Br. Geogr.*, *4*(4), 463-486.

Burbank, B., J. Leland, E. Fielding, R. S. Anderson, N. Brozovic, M. R. Reid, and C. Duncan (1996), Bedrock incision, rock uplift and threshold hillslopes in the northwestern Himalayas, *Nature*, *379*, 505-510.

Coco, G., and A. B. Murray (2007), Patterns in the sand: From forcing templates to self-organization, *Geomorphology*, *91*, 271-290.

Coulthard, T. J., and M. J. Van de Wiel (2007), Quantifying fluvial non linearity and finding self organized criticality?: Insights from simulations of river basin evolution, *Geomorphology*, *91*, 216-235.

Densmore, A. D., M. A. Ellis, and R. S. Anderson (1998), Landslides and the evolution of normal-fault bounded mountains, *J. Geophys. Res.*, *103*(15), 203-215.

Ellis, M. A., and A. L. Densmore (2006), First-order topography over blind thrusts, *GSA Spec. Pap.*, *398*, 251-266.

Ellis, M. A., A. L. Densmore, and R. S. Anderson (1999), Development of mountainous topography in the Basin Ranges, USA, *Basin Res.*, *11*, 21-41.

Fernandes, N. F., and W. E. Dietrich (1997), Hillslope evolution by diffusive processes: The timescale for equilibrium adjustments, *Water Resour. Res.*, *33*(6), 1307-1318.

Fonstad, M. A., and W. A. Marcus (2010), High resolution, basin extent observations and implications for understanding river form and process, *Earth Surf. Processes Landforms*, *35*, 680-698, doi:10.1002/esp.1969.

Gabet, E. J., B. A. Pratt-Sitaula, and D. W. Burbank (2004), Climatic controls on hillslope angle and relief in the Himalayas, *Geology*, *32*, 629-632.

Gardner, T. W. (1983), Experimental study of knickpoint and longitudinal profile evolution in cohesive, homogeneous material, *Geol. Soc. Am. Bull.*, *94*, 664-672.

Gilbert, G. K. (1909), The convexity of hillslopes, *J. Geol.*, *17*, 344-350.
Goren, L., S. D. Willett, F. Herman, and J. Braun (2014), Coupled numerical-analytical approach to landscape evolution modeling, *Earth Surf. Processes Landforms*, *39*, 522-545, doi:10.1002/esp.3514.
Graveleau, F., J. Malavielle, and S. Dominguez (2012), Experimental modelling of orogenic wedges: A review, *Tectonophysics*, *538–540*, 1-66.
Hallet, B. (1990), Spatial self-organization in geomorphology: From periodic bedforms and patterned ground to scale-invariant topography, *Earth Sci. Rev.*, *29*, 57-75.
Hancock, G., and G. Willgoose (2001), The interaction between hydrology and geomorphology in a landscape simulator experiment, *Hydrol. Processes*, *15*, 115-133.
Hasbargen, L. E. (2003), Erosion in steady state drainage basins, PhD thesis, Univ. of Minnesota, Minneapolis.
Hasbargen, L. E., and C. Paola (2000), Landscape instability in an experimental drainage basin, *Geology*, *28*, 1067-1070, doi:10.1130/0091–7613.
Hasbargen, L. E., and C. Paola (2003), How predictable is local erosion rate in eroding drainage basins?, in *Prediction in Geomorphology, AGU Geophys. Monogr. Ser.*, vol. 135, edited by P. Wilcock and R. M. Iverson, pp. 231-240, AGU, Washington, D. C.
Hergarten, S., and H. J. Neugebauer (1998), Self-organized criticality in a landslide model, *Geophys. Res. Lett.*, *25*(6), 801-804.
Horton, R. E. (1945), Erosional development of streams and their drainage basins, *Geol. Soc. Am. Bull.*, *56*, 275-370.
Hovius, N. (1996), Regular spacing of drainage outlets from linear mountain belts, *Basin Res.*, *8*, 29-44.
Hovius, N., C. P. Stark, and P. A. Allen (1997), Sediment discharge from a mountain belt derived by landslide mapping, *Geology*, *25*, 231-234.
Huber, P. J. (1981), *Robust Statistics*, John Wiley, Hoboken, N. J.
Hurst, M. D., M. A. Ellis, K. R. Royse, K. A. Lee, and K. Freeborough (2013), Controls on the magnitude-frequency scaling of an inventory of secular landslides, *Earth Surf. Dyn.*, *1*, 67-78, doi:10.5194/esurf-1–67-2013.
Jerolmack, D. J., and C. Paola (2007), Complexity in a cellular model of river avulsion, *Geomorphology*, *91*, 259-270.
Jerolmack, D. J., and C. Paola (2010), Shredding of environmental signals by sediment transport, *Geophys. Res. Lett.*, *37*, L19401, doi: 10.1029/2010GL044638.
Keiler, M. (2011), Geomorphology and complexity-inseparably connected?, *Z. Geomorphol.*, *55*(3), 233-257.
Korup, O. (2006), Effects of large deep-seated landslides on hillslope morphology, western Southern Alps, New Zealand, *J. Geophys. Res.*, *111*, F01018, doi:10.1029/2004JF000242.
Korup, O., J. J. Clague, R. L. Hermanns, K. Hewitt, A. L. Strom, and J. T. Weidinger (2007), Giant landslides, topography, and erosion, *Earth Planet. Sci. Lett.*, *261*(3–4), 578-589, doi:10.1016/j.epsl.2007.07.025.
Korup, O., A. L. Densmore, and F. Schlunegger (2010), The role of landslides in mountain range evolution, *Geomorphology*, *120*, 77-90, doi: 10.1016/j.geomorph.2009.09.017.
Lague, D., A. Crave, and P. Davy (2003), Laboratory experiments simulating the geomorphic response to tectonic uplift, *J. Geophys. Res.*, *108*(B1), 2008, doi:10.1029/2002JB001785.
Malamud, B. D., and D. L. Turcotte (1999), Self-organized criticality applied to natural hazards, *Nat. Hazards*, *20*, 93-116.
Malamud, B. D., D. L. Turcotte, F. Guzzetti, and P. Reichenbach (2004), Landslide inventories and their statistical scaling properties, *Earth Surf. Processes Landforms*, *29*, 687-711.
Michaelides, K., and M. B. Singer (2014), Impact of coarse sediment supply from hillslopes to the channel in runoff-dominated, dryland fluvial systems, *J. Geophys. Res. Earth Surf.*, *119*, 1205-1221, doi:10.1002/2013JF002959.
Montgomery, D. R., and M. T. Brandon (2002), Topographic controls on erosion rates in tectonically active mountain ranges, *Earth Planet. Sci. Lett.*, *201*, 481-489.
Montgomery, D. R., and W. E. Dietrich (1994), Landscape dissection and drainage area-slope thresholds, in *Process Models and Theoretical Geomorphology*, edited by M. J. Kirkby, pp. 221-246, John Wiley, N. Y.
Murray, A. B. (2007), Two paradigms in landscape dynamics: Self-similar processes and emergence, in *Nonlinear Dynamics in Geoscience*, edited by A. T. Anastasios and J. B. Elsner, pp. 17-35, Springer, N. Y.
Murray, A. B., and M. A. Fonstad (2007), Preface: Complexity (and simplicity) in landscapes, *Geomorphology*, *91*, 173-177.
Murray, A. B., et al. (2009), Geomorphology, complexity, and the emerging science of the Earth's surface, *Geomorphology*, *103*, 496-505.
Paola, C., K. Straub, D. Mohrig, and L. Reinhardt (2009), The "unreasonable" effectiveness of stratigraphic and geomorphic experiments, *Earth Sci. Rev.*, *97*, 1-43.
Parker, R. S. (1977), Experimental study of basin evolution and its hydrologic implications, PhD thesis, Colorado State Univ., Fort Collins.
Passalacqua, P., F. Porté-Agel, E. Foufoula-Georgiou, and C. Paola (2006), Application of dynamic subgrid-scale concepts from large-eddy simulation to modeling landscape evolution, *Water Resour. Res.*, *42*, W06D11, doi:10.1029/2006WR004879.
Pelletier, J. D. (2003), Drainage basin evolution in the Rainfall Erosion Facility: Dependence on initial conditions, *Geomorphology*, *53*, 183-196.
Pelletier, J. D., B. D. Malamud, T. Blodgett, and D. L. Turcotte (1997), Scale-invariance of soil moisture variability and its implications for the frequency-size distribution of landslides, *Eng. Geol.*, *48*, 255-268.
Perron, J. T., W. E. Dietrich, and J. W. Kirchner (2008), Controls on the spacing of first-order valleys, *J. Geophys. Res.*, *113*, F04016, doi: 10.1029/2007JF000977.
Phillips, J. D. (1999), Divergence, convergence, and self-organization in landscapes, *Ann. Assoc. Am. Geogr.*, *89*(3), 466-488.
Rodriguez-Iturbe, I., and A. Rinaldo (1997), *Fractal River Basins: Chance and Self Organization*, Cambridge Univ. Press, Cambridge, U. K.
Rohais, S., S. Bonnet, and R. Eschard (2012), Sedimentary record of tectonic and climatic erosional perturbations in an experimental coupled catchment-fan system, *Basin Res.*, *24*, 198-212, doi:10.1111/j.1365–2117.2011.00520.x.
Sapozhnikov, V. B., and E. Foufoula-Georgiou (1996), Do the current landscape evolution models show self-organized criticality?, *Water Resour. Res.*, *32*(4), 1109-1112.
Sapozhnikov, V. B., and E. Foufoula-Georgiou (1997), Experimental evidence of dynamic scaling and indications of self-organized criticality in braided rivers, *Water Resour. Res.*, *33*(8), 1983-1991.
Schumm, S. A., M. P. Mosley, and W. E. Weaver (1987), *Experimental Fluvial Geomorphology*, John Wiley, N. Y.
Singh, A., L. Reinhardt, and E. Foufoula-Georgiou (2015), Landscape re-organization under changing climatic forcing: Results from an experimental landscape, *Water Resour. Res.*, doi:10.1002/2015WR017161, in press.
Stark, C., and N. Hovius (2001), The characterization of landslide size distributions, *Geophys. Res. Lett.*, *28*(6), 1091-1094.
Summerfield, M. A., and N. J. Hulton (1994), Natural controls of fluvial denudation rates in major world drainage basin, *J. Geophys. Res.*, *99*(B7), 13,871-13,883.

Talling, P. J., M. D. Stewart, C. P. Stark, S. Gupta, and S. J. Vincent (1997), Regular spacing of drainage outlets from linear faults blocks, *Basin Res.*, *9*, 275-302.

Van de Wiel, M. J., and T. J. Coulthard (2010), Self-organized criticality in river basins: Challenging sedimentary records of environmental change, *Geology*, *38*(1), 87-90, doi:10.1130/G30490.1.

Werner, B. T. (1995), Eolian dunes: Computer simulations and attractor interpretation, *Geology*, *23*(12), 1107-1110.

Werner, B. T. (1999), Complexity in natural landform patterns, *Science*, *284*, 102-104.

Whipple, K. X. (2004), Bedrock rivers and geomorphology of active orogens, *Annu. Rev. Earth Planet. Sci.*, *32*, 151-185.

Whipple, K. X., E. Kirby, and S. Brocklehurst (1999), Geomorphic limits to climatically induced increases in topographic relief, *Nature*, *401*, 39-43.

Willett, S. D., S. W. McCoy, J. T. Perron, L. Goren, and C.-Y. Chen (2014), Dynamic reorganization of river basins, *Science*, *343*, 1248765, doi: 10.1126/science.1248765.